AIAA JOURNAL
Vol. 38, No. 5, May 2000

Oscillation of Vortex Breakdown Location and Blowing Control of Time-Averaged Location

Anthony M. Mitchell,* Didier Barberis,† Pascal Molton,‡ and Jean Délery§
ONERA, 92190 Meudon, France

The goal of this research is the control of leading-edge vortex breakdown location utilizing along-the-core blowing near the apex on the leeward surface of sharp-edged, slender, delta wings at high angles of attack. In the S2Ch subsonic wind tunnel at ONERA Chalais–Meudon, two delta wing models with 70-deg sweep angles and root chords of 950 mm have been configured to collect qualitative and quantitative surface and flowfield data. First, an examination of the streamwise, time-dependent oscillation of the leading-edge vortex breakdown locations without active flow control is presented. These results further the understanding of the vortex breakdown phenomena and provide a more precise basis for evaluating the effectiveness of various flow control methods. Second, open-loop blowing along one of the vortex cores on the leeward surface of the delta wing demonstrates the ability to displace downstream the controlled, time-averaged, vortex breakdown location by 20% of the root chord.

Nomenclature

b	= wingspan
C_p	= pressure coefficient
C_μ	= momentum coefficient, $Q_m V_j / q_\infty S$
c	= root chord length
f	= frequency
Q_m	= blowing mass flow rate
q_∞	= dynamic pressure
Re_c	= Reynolds number with respect to root chord
S	= wing area
Sr	= Strouhal number, fc/U_∞
U_∞	= freestream velocity
V_j	= jet exit velocity
X_b	= vortex breakdown location from wing apex
X_b/c	= nondimensional vortex breakdown location
Y/b	= nondimensional wing span location
α	= angle of attack
Λ	= sweep angle

Introduction

THE development of extremely maneuverable fighter aircraft and missiles has resulted in flight regimes that involve high angles of attack, raising interest in the study of three-dimensional separated flows. The delta wing design has become the prominent configuration used by manufacturers of combat aircraft worldwide, such as Lockheed's F-117, Dassault's Rafale, the Eurofighter, and Boeing's design for the Joint Strike Fighter. A distinguishing feature of the delta wing flowfield, at moderate to high angles of attack, is the formation of several vortical structures on the leeward surface. These vortical structures result from the rolling up of the viscous flow sheet previously confined within the boundary layer attached to the leeward surface.[1] The most prominent of these vortical structures, which form along the sharp leading edges of delta wings, are called *leading-edge vortices*. The axial velocity component in the leading-edge vortex core can reach values as high as three times the freestream velocity.[2] The vortex dynamics are influenced by several delta wing parameters, which include sweep angle, leading-edge geometry, and wing thickness, as well as freestream conditions and angle of attack.[2] These leading-edge vortices produce between 30 and 60% of the total lift at high α (Ref. 3). Therefore, delta wings have a significant advantage in lift forces when compared with other wing designs. However, at high α, these well-organized leading-edge vortices often experience a sudden disorganization, known as *vortex breakdown*.

Different theories governing vortex breakdown have been proposed, although none has been universally accepted.[4–8] Several types of vortex breakdown have been identified (including the predominant spiral and axisymmetric bubble), and all are followed by a region of recirculating and highly turbulent flow.[6] In general, the vortex breakdown phenomenon can be characterized by a rapid deceleration of both the axial and swirl components of the mean velocity and, at the same time, a dramatic expansion of the vortex core.[8] During the breakdown process, the mean axial velocity component rapidly decreases until it reaches a stagnation point and/or becomes negative on the vortex axis. This stagnation point, known as the *breakdown location*, is unsteady and typically oscillates about some mean position.[7] As α is increased, the vortex breakdown location moves upstream over the delta wing (from the trailing edge toward the apex).

In 1954, Werlé published water-tunnel results in which he first visualized vortex breakdown on the leeward surface of a delta wing.[9] These results were confirmed by Peckham and Atkinson[10] in 1957 and by Elle[11] in 1960. Since then, numerous theoretical, experimental, and computational studies have been published concerning the physics of vortical flow, vortex breakdown, and control of vortex breakdown. Werlé[12] was the first to attempt to control the vortex breakdown location. Initially, he observed the effects of placing an obstacle downstream of the trailing edge of a delta wing and then implemented a system of suction in the core of the leading-edge vortex and in the recirculating region behind the vortex breakdown. He also examined the influence of a jet blowing in the direction of the vortex core. (The jet was situated on the windward side of the delta wing.) Werlé and Gallon,[13] as well as Poisson-Quinton,[14] extended this study to include blowing along the vortex core with a jet on the leeward side of the delta wing. Since these early studies, further research has been conducted utilizing blowing along the leading-edge vortex cores of delta wings or parallel to the leading edge of the wing.[15–28] The current research is a continuation of earlier studies[24,25] at ONERA examining open-loop, along-the-core blowing as a method of manipulating the vortex breakdown location. Neglected in these previous efforts was the importance of the time-dependent, oscillating vortex breakdown locations, which affect the evaluation of flow control methods. Several authors have discussed these nonlinear instabilities and the asymmetry of vortex breakdown locations.[29–38] Gursul and Yang,[35] Menke et al.,[36] and Menke and

Received 29 April 1998; presented as Paper 98-2914 at the AIAA 29th Fluid Dynamics Conference, Albuquerque, NM, 15–18 June 1998; revision received 29 January 1999; accepted for publication 24 August 1999.

*Research Engineer, Fundamental and Experimental Aerodynamics Department. Member AIAA.
†Chief Engineer, Fundamental and Experimental Aerodynamics Department.
‡Engineer, Fundamental and Experimental Aerodynamics Department.
§Head, Fundamental and Experimental Aerodynamics Department. Senior Member AIAA.

Report Documentation Page

Form Approved
OMB No. 0704-0188

1. REPORT DATE	2. REPORT TYPE	3. DATES COVERED
00 MAY 2000	**N/A**	**-**

4. TITLE AND SUBTITLE	5a. CONTRACT NUMBER
Oscillation of Vortex Breakdown Location and Blowing Control of Time-Averaged Location	5b. GRANT NUMBER
	5c. PROGRAM ELEMENT NUMBER
6. AUTHOR(S)	5d. PROJECT NUMBER
	5e. TASK NUMBER
	5f. WORK UNIT NUMBER
7. PERFORMING ORGANIZATION NAME(S) AND ADDRESS(ES) **United States Air Force Academy, Department of Aeronautics 2410 Faculty Drive, USAF Academy, CO 80840, USA**	8. PERFORMING ORGANIZATION REPORT NUMBER
9. SPONSORING/MONITORING AGENCY NAME(S) AND ADDRESS(ES)	10. SPONSOR/MONITOR'S ACRONYM(S)
	11. SPONSOR/MONITOR'S REPORT NUMBER(S)

12. DISTRIBUTION/AVAILABILITY STATEMENT
Approved for public release, distribution unlimited

13. SUPPLEMENTARY NOTES
See also ADM001662.

14. ABSTRACT

15. SUBJECT TERMS

16. SECURITY CLASSIFICATION OF:			17. LIMITATION OF ABSTRACT	18. NUMBER OF PAGES	19a. NAME OF RESPONSIBLE PERSON
a. REPORT	b. ABSTRACT	c. THIS PAGE			
unclassified	**unclassified**	**unclassified**	**UU**	**11**	

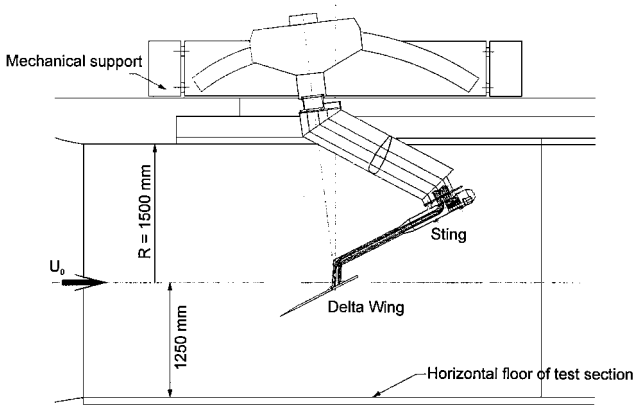

Fig. 1 Experimental configuration in S2Ch.

Gursul[37] described the fluctuations of vortex breakdown locations in water at Re_c from 4.0×10^4 to 5.5×10^4. No previously published materials have been identified that describe the streamwise oscillation of the vortex breakdown locations at the Re_c examined during this effort (9.75×10^5 to 2.6×10^6).

The primary goal of this work is to characterize the streamwise time-dependent oscillations of the vortex breakdown at these higher Reynolds numbers and to relate them to previous studies accomplished at lower Reynolds numbers. These results expand the general knowledge of the phenomena and provide a more precise basis for evaluating the effectiveness and for understanding the influences of the flow control methods. Second, experimental results of blowing along one of the vortex cores on the leeward surface of the delta wing are presented as a method of manipulating the vortex breakdown locations.

Wind Tunnel

This study was accomplished in the S2Ch subsonic wind tunnel at ONERA's Chalais–Meudon center. The test section of S2Ch is quasicircular, with a diameter of 3 m, a length of 5 m, and a horizontal floor with a width of 1.6 m. The wind tunnel is powered by a 1500-kW motor that provides a maximum $U_\infty = 120$ m/s at atmospheric conditions. It is currently operated at freestream velocities between 10 and 100 m/s (Reynolds numbers with respect to the diameter of the test section between 2×10^6 and 20×10^6). The velocity can be stabilized to within $\pm 0.2\%$ of the desired velocity up to the maximum freestream velocity. The mean intensity of turbulence in S2Ch is 0.2%.

The delta wing models were mounted on a sting protruding from the upper surface of the test section, with their leeward surface pointing down, toward the floor (Fig. 1). The angle of attack is measured to within ± 0.1 deg. The models were mounted in the test section with no yaw angle with respect to the freestream flow. All of the tubing for the pressure taps and for compressed air was contained within the sting that connected the models to the mechanical support used for adjusting α in the test section. The compressed-air system is capable of providing a maximum pressure of 40×10^5 Pa at a temperature of 300 K and at a mass flow rate of 2 kg/s.

Models

Two delta wing models with 70-deg sweep angles Λ and root chords c of 950 mm were configured to collect qualitative and quantitative surface and flowfield data during these tests. Each model has a wingspan of 691.5 mm at its trailing edge, is 20 mm thick, and is beveled on the windward side at an angle of 15 deg to form sharp leading edges (Fig. 2).

Both models are equipped with a nozzle for along-the-core blowing on the portside of the wing. The nozzle configuration consists of a circular jet with an interior diameter of 2.07 mm, which expands into an open duct at an angle of 15.6 deg with respect to the leeward surface of the wing (Fig. 3). The nozzle is located 14% of the root chord behind the apex of the wing and is situated 30 mm from the portside leading edge. The various total pressures of the upstream compressed air and therefore the blowing mass flow rates discussed

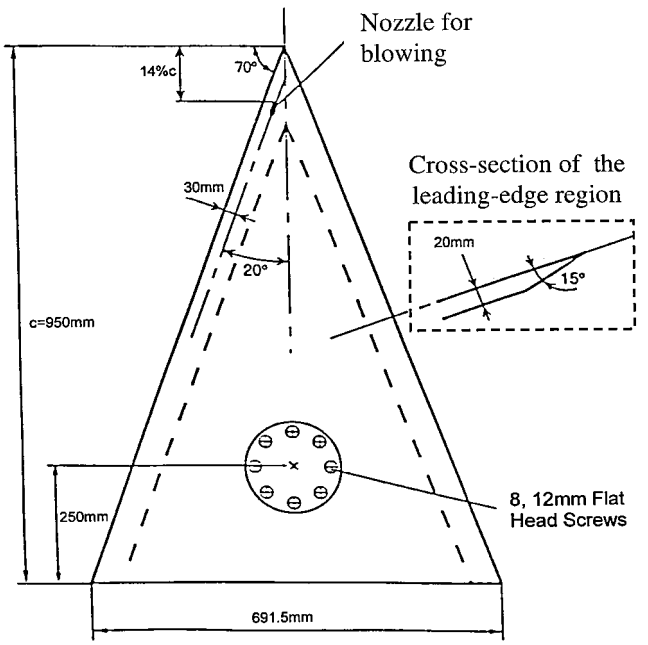

Fig. 2 Diagram of the model.

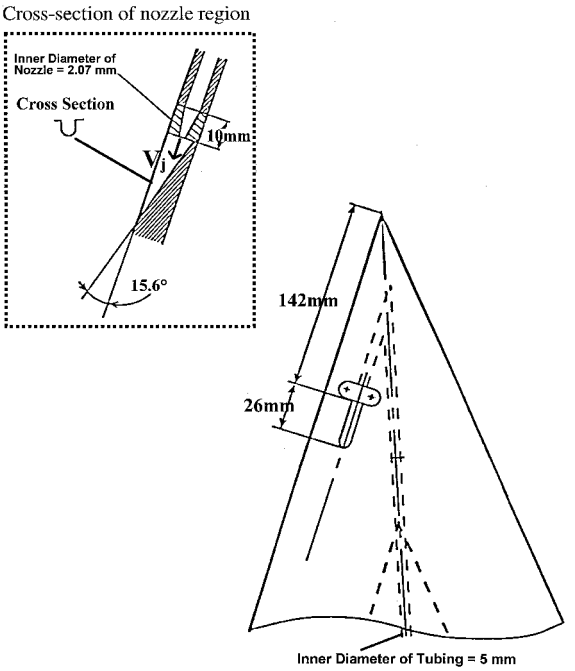

Fig. 3 Configuration for blowing.

in this paper all result in sonic jet exit velocities V_j based on the isentropic relations. The position of the nozzle close to the leading edge and near the apex along the leeward surface was reported to be an optimal position for maximizing control and minimizing the blowing mass flow rate.[20] The jet of compressed air exits the nozzle slightly inward of the portside vortex core (less than 5 deg), which corresponds closely to the optimal orientation presented by Guillot et al.[28]

The model without surface instrumentation was used to obtain qualitative flowfield visualization data and surface oil flow data. The second, geometrically identical, model with 232 steady pressure taps was used to collect time-averaged surface pressure data. The pressure taps are 2 mm in diameter and are situated in 16 transverse sections normal to the root chord. The first row is 100 mm behind the apex. Beginning with the second row of pressure taps, 200 mm aft of the apex, all of the other 15 rows are spaced at 50-mm intervals along the chord, with the final row being 900 mm downstream of the apex. Various numbers of pressure taps traverse the full span

of the wing at each chordwise location, depending on the distance downstream.

Data Acquisition

Flowfield visualization using laser sheet techniques was implemented in three directions: in the plane intersecting the two leading-edge vortex cores above the leeward surface of the delta wing and perpendicular to the leeward surface of the model both parallel and normal to the root chord. All laser sheet flow visualizations were accomplished with a 15-W argon laser. The beam was diffracted around a cylinder and oriented in the test section by a number of mirrors, which permitted adjustment of the elevation and rotation of the laser sheet. Theater smoke (P/Smog FS25) was generated in a commercial smoke machine and then entrained into the flow upstream of the wind tunnel's collector. Both the elevation and the orientation of the smoke were adjusted to maximize flow visualization. The results were captured on videotape by using a Sony digital video camera, placed perpendicular to the model's leeward surface, which recorded images at a rate of 50 frames/s.

Although purely qualitative in nature, laser sheet flow visualization shows the development of the leading-edge vortices on the leeward surface of the delta wing and allows for time-dependent identification of the vortex breakdown location. The two laser sheet views normal to the wing were used to identify the location of the vortex cores above the leeward surface of the wing. The angle between the model and the laser sheet aligned with the vortex core remained constant throughout all of the test conditions (approximately 7 deg).

Of specific interest are the flow visualization results from the laser sheet aligned with both of the leading-edge vortex cores, which reveal the streamwise oscillation of the portside and starboard vortex breakdown locations at the same instant in time. The streamwise distances of the breakdown locations (portside and starboard) from the apex of the delta wing (X_b) were measured directly from the recorded images. These values were then divided by the root chord length c of the delta wing measured from the video images, resulting in a nondimensional length X_b/c. Because both lengths were measured from the video data, the small angle between the model and the laser sheet was neglected. Measurement uncertainty of the distances obtained is estimated to be of the order of $0.01c$.

The lowest resolvable frequency of the measured oscillations of the vortex breakdown location is related to the total length of the time history examined. Therefore, a longer time history will enable smaller minimum frequencies $f_{\min}$. However, as the length of the time history increases, the number of data points also increases, forcing a compromise. A time history of approximately 60 s was chosen, which corresponds to Strouhal numbers Sr equal to 0.00106, 0.00066, and 0.0004, respectively, for $U_\infty = 15$, 24, and 40 m/s. The highest frequency $f_{\max}$ of resolution is directly related to the frame speed of the video camera; however, no major difference in the principal frequencies of the oscillating vortex breakdown locations was noticed for data analyzed at 50 and 25 frames/s. Therefore, the video data were evaluated at 25 frames/s. Thus, the maximum frequency that can be resolved is $f_{\max} = 12.5$ Hz, corresponding to $Sr = 0.792$, 0.495, and 0.297, respectively, for the three freestream velocities.

Steady (time-averaged) surface pressure data were obtained by using the pressure model in conjunction with a Scanivalve system consisting of 13 analog data channels. Six of the channels returned steady surface pressure data, whereas the other seven recorded position, α, and pertinent freestream conditions. Five hundred measurements were acquired, at 7 kHz, for each channel before the Scanivalve system was advanced, stabilized, and recycled to capture data from the next six pressure taps. The steady surface pressure values were computed from these data and are plotted with respect to their location on the wing. No blockage, wall, or wake corrections were made to the data.

Surface oil flow visualization was accomplished with a viscous coating composed of a mixture of 60% paraffin oil and 40% zinc titanium (percentage based on the mass of the oil). The leeward surface of the delta wing was covered with a thin layer of the oil–zinc mixture, and the wind tunnel was operated to achieve each test condition. Skin friction and surface effects caused the coating to build up in certain areas and to diffuse in others. Surface oil flow photographs of the delta wing were taken at each U_∞ and α with and without tangential blowing. One can interpret the topology of the oil streaks to understand better the relationship between the vortices and the surface skin friction pattern through the use of the critical point theory.[39]

Results

Time-Dependent Oscillation of Vortex Breakdown Location

Previous research has shown that breakdown locations of leading-edge vortices over stationary wings at high α are not steady but oscillate in the streamwise direction.[7,29–38] None of these studies examined the frequencies of the oscillating vortex breakdown locations at the Reynolds numbers presented here. Therefore, these results examining the time history of the oscillations and the resulting principal frequencies will supplement data available for characterizing the time-dependant nature of the vortex breakdown phenomenon.

The no-blowing configuration $C_\mu = 0$ of the delta wing was examined for $U_\infty = 15$, 24, and 40 m/s at $\alpha = 20$, 27, 30, and 40 deg. The Reynolds numbers associated with each U_∞ are, respectively, $Re_c = 9.75 \times 10^5$, 1.56×10^6, and 2.6×10^6. Using the laser sheet flowfield visualization techniques discussed earlier, plots were made of the portside and starboard nondimensional vortex breakdown locations X_b/c vs time for all of the test conditions. At $\alpha = 20$ deg, the breakdown locations were, for all freestream velocities, aft of the trailing edge of the delta wing. At $\alpha = 27$, 30, and 40 deg, the breakdown locations oscillated over the leeward surface of the delta wing. For conciseness, only a portion of the total data obtained is discussed here.

The portside and starboard X_b/c data vs time for a period of approximately 60 s are presented in Figs. 4 and 5. A black line identifies the portside vortex breakdown locations, and a gray line connects the starboard vortex breakdown locations. Three plots representing data obtained at $\alpha = 27$ deg are contained in Fig. 4; Fig. 5 shows data at $\alpha = 30$ deg. Each of the individual plots represents a test condition with a different freestream velocity. Whereas Figs. 4 and 5 provide a global perspective of the oscillation of the vortex breakdown, Fig. 6 is a graph of the time-averaged, portside and starboard, X_b/c values calculated from the approximately 1500 data points shown in Figs. 4 and 5. The root-mean-square (rms) values of the oscillating breakdown locations for each of the test conditions are also included in Fig. 6. To facilitate the interpretation of the data, lines connect the corresponding portside and starboard mean vortex breakdown locations.

The data obtained for the test case at $\alpha = 27$ deg and $U_\infty = 40$ m/s demonstrate the sensitivity of the breakdown location to external factors. All of the data presented were very repeatable, with mean X_b/c changing only slightly for different test runs on different days and during different runs of the wind tunnel. The data at $\alpha = 27$ deg and $U_\infty = 40$ m/s tended to be more random, and their mean breakdown location in Fig. 6 falls outside the range of the other data at the same angle of attack. Also note that the rms values for this test condition were well above the other values. There is no direct indication as to what created this discrepancy during the testing, and the same type of behavior was not observed at $\alpha = 30$ deg and $U_\infty = 40$ m/s as one might expect if the effects were due to the higher freestream velocities.

The negligible influence of varying U_∞ on the vortex breakdown locations while α remains fixed is shown in both Figs. 4 and 5. Additionally, the rms values of the time-averaged breakdown locations shown in Fig. 6 indicate that changing the freestream velocity has little impact on the oscillating vortex breakdown locations. However, comparing like plots between Figs. 4 and 5, one can easily observe the influence of α on the breakdown locations, whereas U_∞ remains constant. As α increases, the trend is for X_b/c to move forward, toward the apex of the delta wing, and this change is accompanied by a reduction in the amplitude of the oscillations of the vortex breakdown locations. Thus, increasing α stabilizes the vortex breakdown locations, as is evident from the decreasing rms values at corresponding test conditions in Fig. 6. Increasing the angle of

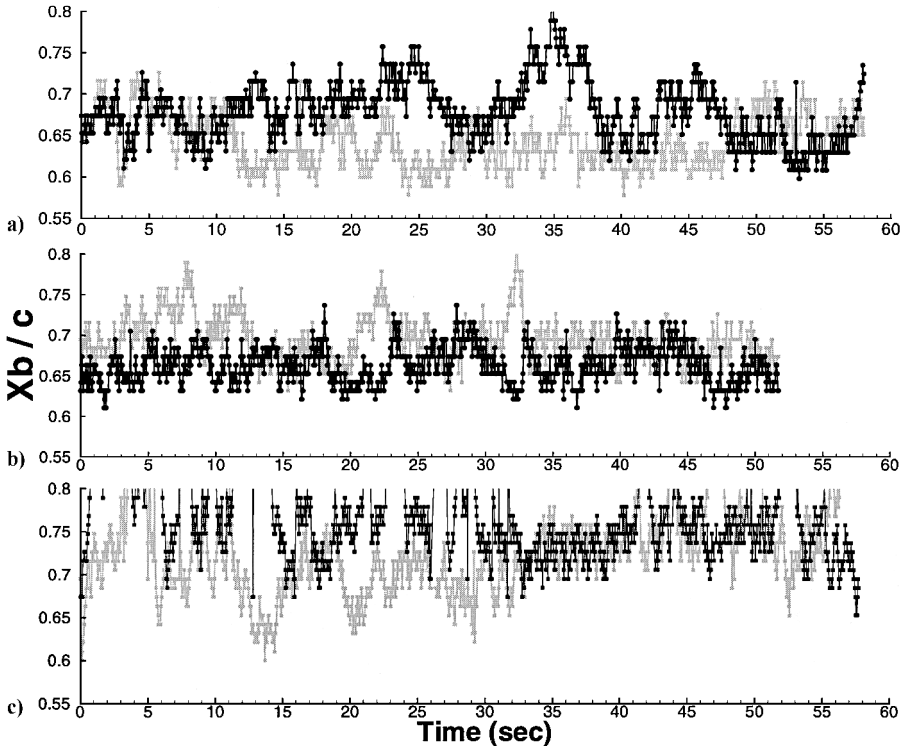

Fig. 4 X_b/c vs time at $\alpha = 27$ deg; no flow control: a) $U_\infty = 15$ m/s, b) $U_\infty = 24$ m/s, and c) $U_\infty = 40$ m/s.

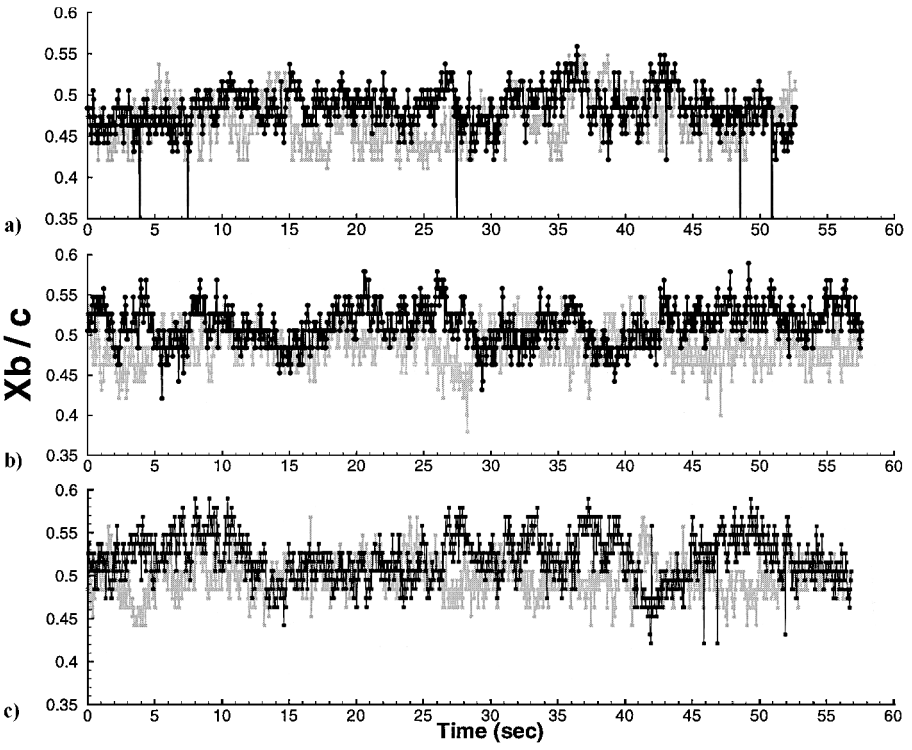

Fig. 5 X_b/c vs time at $\alpha = 30$ deg; no flow control: a) $U_\infty = 15$ m/s, b) $U_\infty = 24$ m/s, and c) $U_\infty = 40$ m/s.

attack adds energy to the leading-edge vortices as a result of increased adverse pressure gradients producing higher axial and swirl velocities than at lower incidence angles. These trends confirm results described in previous vortex breakdown studies.

The data also indicate an interaction between the two leading-edge vortices, which causes the vortex breakdown locations on each side of the wing to oscillate out of phase. As the breakdown location on one side of the delta wing moves aft, the other tends to move forward and vice versa. In some instances, the oscillations are 180 deg out of phase, indicating strong interactions between the leading-edge vortices.

The oscillations of X_b/c in Figs. 4 and 5 occur at both a high frequency with low amplitude and at a low frequency with high amplitude. To understand further the oscillating phenomenon, the power spectrum of the X_b/c vs time data has been analyzed to determine the makeup of these frequencies. The power spectral density (PSD) of each set of data examined in Figs. 4 and 5 was determined by using Fourier transform spectral methods. The discrete Fourier

transform of the data was computed using a standard fast Fourier transform (FFT) routine. A periodogram estimate of the power spectrum was then obtained by using a Welch window.[40]

A sample of the principal PSD peak frequencies, in terms of Strouhal number, is shown in Table 1 for various test conditions in S2Ch without flow control, along with a bar graph that represents the range of observed values throughout all of the test conditions (Fig. 7). The lowest and highest principle peak frequencies, 0.0424 and 0.0697, respectively, represent the inclusive range of the graph. The low-frequency, high-amplitude frequencies returned the largest PSD results and not the high-frequency, low-amplitude oscillations. The current test results have been superimposed over the results presented by Menke et al.[36] that were obtained from data observed at much lower Reynolds numbers (Fig. 7). The Strouhal number range identified by Menke et al. as the fluctuation frequencies of vortex breakdown locations over the delta wing spans from 0.057 to 0.095. The current results fall close to or within this range (Fig. 7). The coincidence of the oscillating frequencies of the vortex breakdown location data at two different Reynolds numbers demonstrates that Reynolds number does not strongly influence the oscillating vortex breakdown phenomena. These quantitative data confirm the results observed from qualitative flow visualization data[7] and justify comparison of the vortex breakdown behavior over delta wings at various freestream velocities, both experimentally and in various numerical simulations.

Time-Averaged Surface Pressure

The time-dependent oscillation of the vortex breakdown locations cannot be captured with steady surface pressure taps resulting in time-averaged data. However, the time-averaged surface pressure data may be useful in better understanding the vortex breakdown phenomena. Additionally, if the steady pressure data can be shown to be a reliable indicator of the mean vortex breakdown location, they could be used as an inexpensive feedback mechanism for a closed-loop control system.

Two representative plots of the steady surface pressure results for the no-blowing case are shown in Fig. 8. The leeward surface of the wing is shown as a black region over which all other data are superimposed. The locations of the 232 steady pressure taps are indicated by black squares. The time-averaged pressure coefficients C_p for each of the pressure taps were linearly triangulated over the leeward surface of delta wing and are plotted as constant pressure coefficient regions at $U_\infty = 24$ m/s for $\alpha = 27$ and 30 deg, respectively. The peak negative pressure coefficients at each chordwise location correspond, more or less, to the location of the leading-edge vortex cores and, thus, have been connected by lines to indicate their position in Fig. 8.

These plots are indicative of the general trend observed from all of the time-averaged C_p data: the magnitude of the suction peaks are a maximum at the apex of the wing, with a decreasing magnitude and a broadening of the constant C_p regions toward the trailing edge. Comparing the two plots of Fig. 8, one observes the influence on C_p of increasing the angle of attack: the magnitude of the suction peak increases along the core as α increases. Although there are differences in the size and shape of the constant pressure coefficient lines at various angles of attack, the peak negative pressure coefficients of the steady surface pressure data in Fig. 8 do not clearly indicate the time-averaged vortex breakdown locations on the leeward surface of the model. From the time-averaged visualization data at $U_\infty = 24$ m/s, we know that the mean vortex breakdown locations occur in the vicinity of $X_b/c = 0.65$ at $\alpha = 27$ deg and near $X_b/c = 0.5$ at $\alpha = 30$ deg (Fig. 6). Small discrepancies in the steady pressure data exist in these regions; however, there is not sufficient evidence to indicate that changes in the peak-pressure-coefficient data correspond to the vortex breakdown locations at each respective angle of attack.

Table 1 Fluctuations of breakdown location (see Fig. 7)

Test condition	Portside principal peak, *Sr*	Starboard principal peak, *Sr*
$\alpha = 27$ deg, $U_\infty = 15$ m/s	0.0677	0.0697
$\alpha = 27$ deg, $U_\infty = 24$ m/s	0.0424	0.0435
$\alpha = 27$ deg, $U_\infty = 40$ m/s	0.0456	0.0456
$\alpha = 30$ deg, $U_\infty = 24$ m/s	0.0443	0.0483

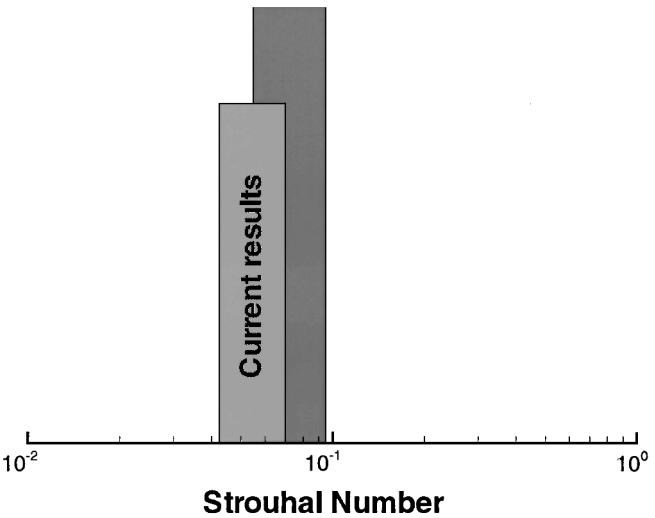

Fig. 7 Fluctuations of breakdown location: current results superimposed on the results of Menke et al.[36] (see Table 1).

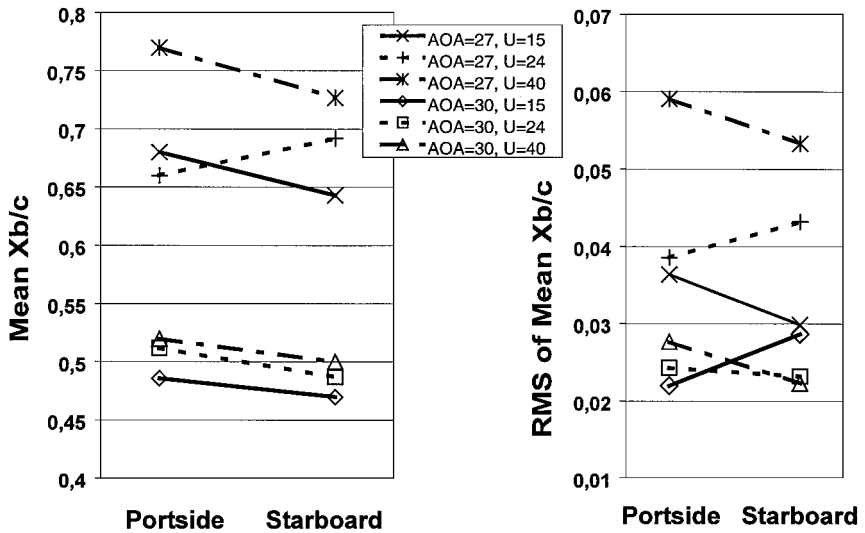

Fig. 6 Time-averaged breakdown location and rms values: no flow control.

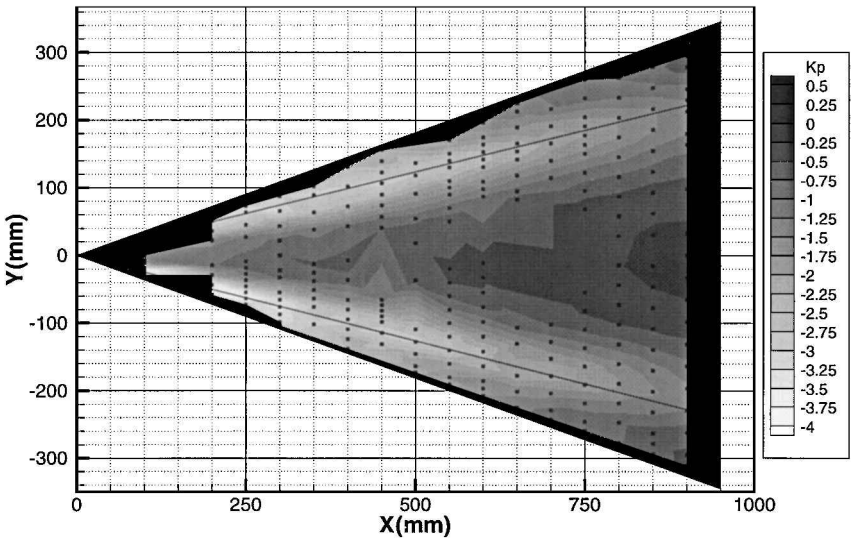

$\alpha = 27$ deg

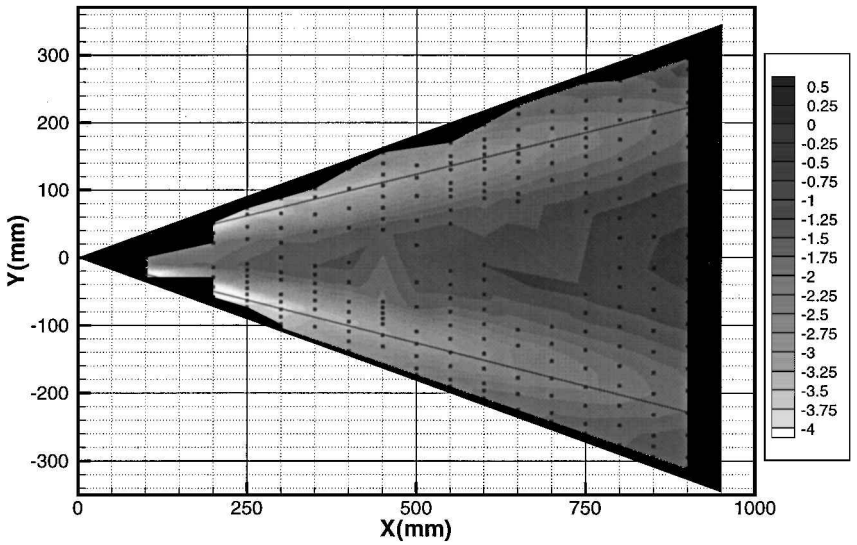

$\alpha = 30$ deg

Fig. 8 Lines of constant-pressure coefficient on the leeward surface at $U_\infty = 24$ m/s; no flow control.

Greenwell and Wood[41] demonstrated the ability of steady surface pressure measurements to identify the vortex breakdown locations over delta wings using the half-width of the peak pressure coefficients in lieu of the peak values of C_p. The width of the pressure coefficient contours does change in the vicinity of the mean vortex breakdown locations in both plots of Fig. 8, but the trend is not consistent throughout the data in these experiments. In some cases, the current results agree with Greenwell and Wood's findings and show a dramatic change in the half-width of the peak pressure coefficients in the vicinity of the mean vortex breakdown location. For other cases, there is no change in the half-width of the peak C_p near the mean breakdown location. Thus, no conclusions can be drawn from these data, except that the steady surface pressure measurements are not a reliable tool for indicating the time-averaged vortex breakdown location on the leeward surface of the delta wing.

On the other hand, a recent study by Jupp et al.[42] showed that unsteady surface pressure measurements can be used to identify the leading-edge vortex breakdown locations. Again, the peak values of C_p from the unsteady pressure measurements were not used, but the rms values of the pressure deviations around the mean value of C_p showed trends that closely correlated with visualization data of vortex breakdown location. Unsteady surface pressure measurements are more expensive than steady pressure measurements, but if they result in more accurate indications of the breakdown location they could be implemented as a feedback mechanism for a closed-loop control system. Future tests will be accomplished to incorporate unsteady pressure measurements on the delta wing model to validate these results.

Surface Oil Flow Visualization

Another way to confirm the surface pressure data results is to analyze the influence of leading-edge vortices on the delta wing's surface by using surface oil flow visualization. If sufficient time-averaged vortex/surface interactions exist in the breakdown regions, this could lead to a better understanding of the steady surface pressure results. The surface oil flow results, without flow control, indicate the time-averaged separation and attachment lines of the leading-edge vortices on the leeward surface of the delta wing. The sharp leading edges of the delta wing force the primary separation lines to coincide with each leading edge. The two leading-edge vortices interact above the root chord and reattach to the wing surface. Along the secondary separation lines near the apex of the delta wing, a transition zone, from laminar to turbulent flow, turned the oil flow pattern outward, toward the leading edges. Secondary attachment lines were observed between the primary and secondary separation lines. These results confirm the result shown by Délery[1,8]; however, the surface oil flow patterns do not denote any trace of the vortex breakdown occurring over the leeward surface of the

delta wing. This supports the conclusion drawn from the steady surface pressure results that time-averaged surface measurements are not a reliable method of identifying the mean vortex breakdown locations.

Open-Loop, Along-the-Core Blowing

The influence of open-loop, along-the-core blowing, near the apex on the leeward surface of a delta wing, was examined as a method of controlling the vortex breakdown locations. In this study, blowing mass flow rates were varied along the axis of the portside leading-edge vortex of the leeward surface of the wing. Momentum coefficients C_μ are used to compare the different blowing mass flow rates at various freestream conditions. As in the nominal case without blowing, the delta wing was examined for U_∞ = 15, 24, and 40 m/s at α = 27, 30, and 40 deg ($Re_c = 9.75 \times 10^5$, 1.56×10^6, and 2.6×10^6).

By using laser sheet flowfield visualization techniques discussed earlier, plots of X_b/c data vs time were compiled for various C_μ. For conciseness, only the results at α = 27 deg and U_∞ = 15, 24, and 40 m/s are discussed. It is important to relate the results seen in Figs. 9–11, with flow control, to those of Fig. 4, which contains plots at the same freestream conditions without blowing.

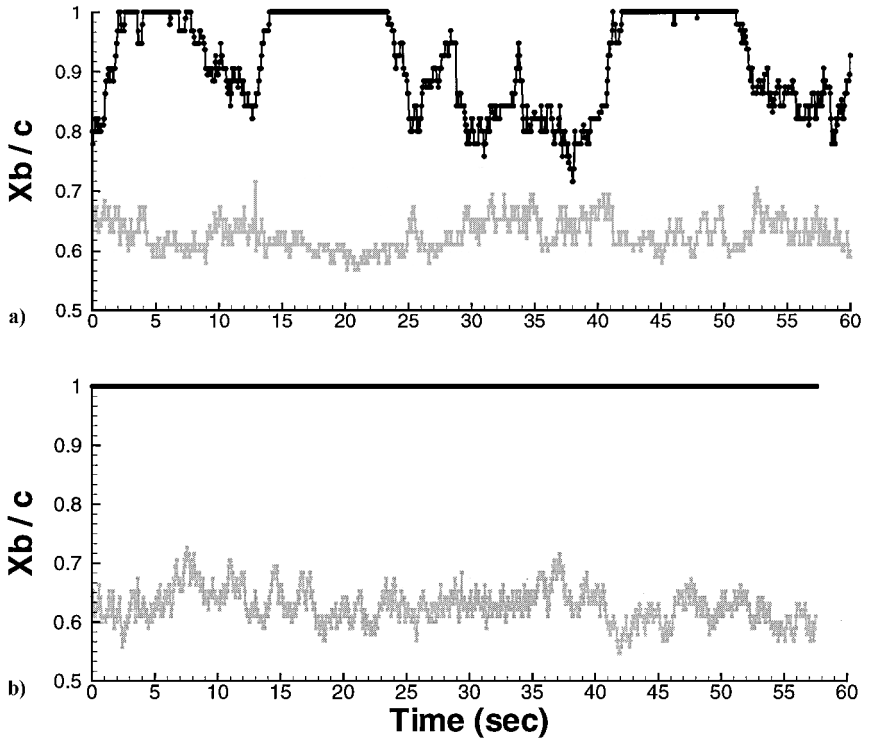

Fig. 9 Time-averaged breakdown location vs time at α = 27 deg for U_∞ = 15 m/s: a) C_θ = 0.009 and b) C_θ = 0.03.

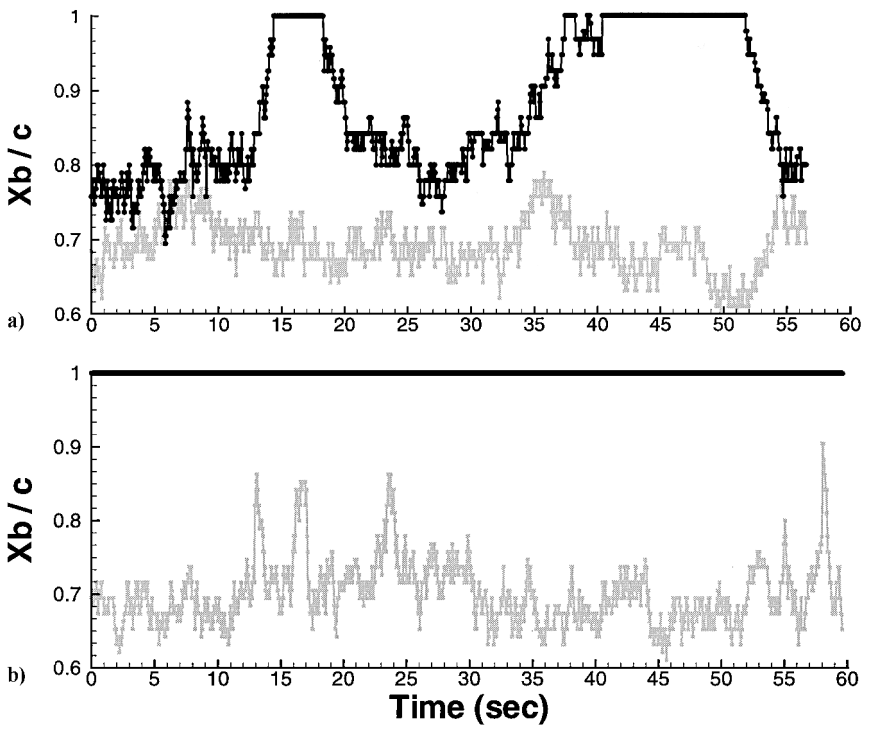

Fig. 10 Time-averaged breakdown location vs time at α = 27 deg for U_∞ = 24 m/s: a) C_θ = 0.005 and b) C_θ = 0.009.

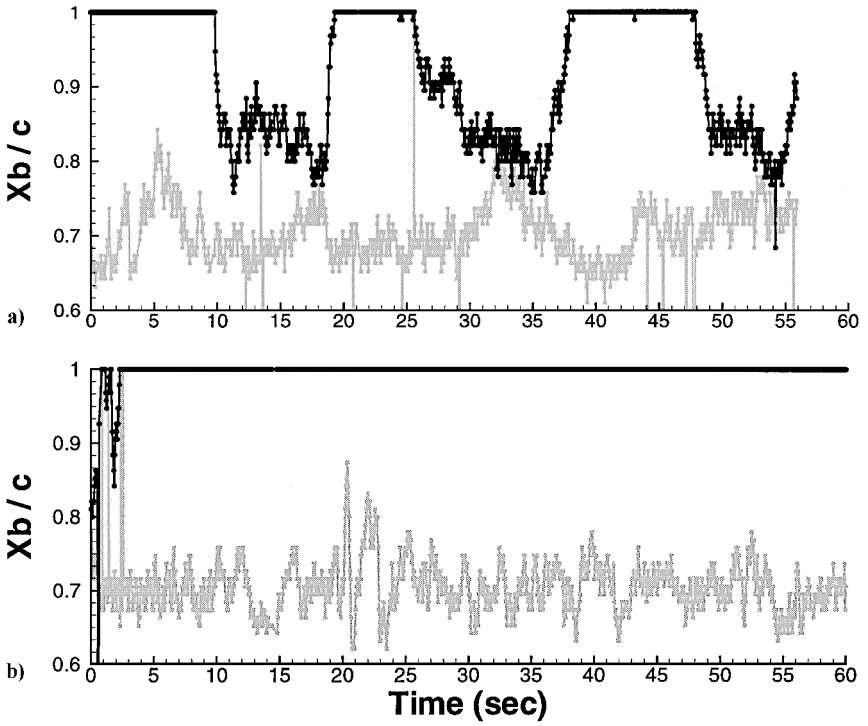

Fig. 11 Time-averaged breakdown location vs time at $\alpha = 27$ deg for $U_\infty = 40$ m/s: a) $C_\theta = 0.0032$ and b) $C_\theta = 0.0036$.

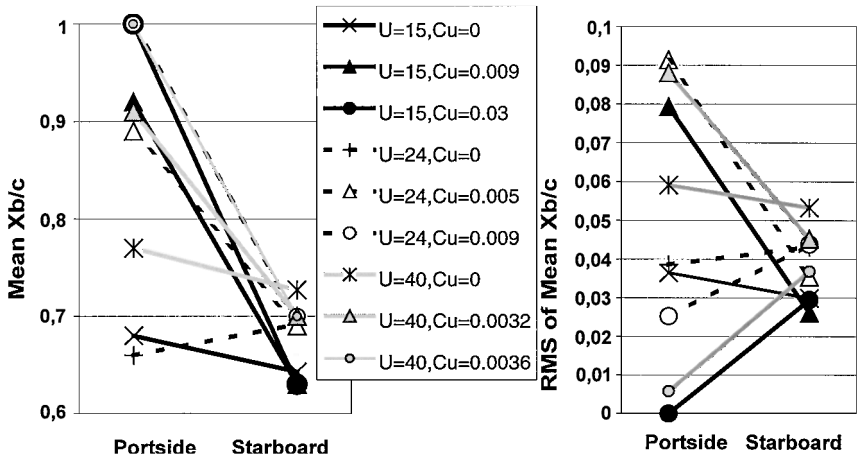

Fig. 12 Time-averaged breakdown location and rms values with and without flow control at $\alpha = 27$ deg.

Two plots representing data obtained at $\alpha = 27$ and $U_\infty = 15$ m/s for blowing momentum coefficients of 0.009 and 0.03 are shown in Fig. 9. These C_μ values correspond to blowing mass flow rates of 1.4 and 3.3 g/s, respectively. Plots of data at $U_\infty = 24$ m/s with $C_\mu = 0.005$ and 0.009 ($Q_m = 1.8$ and 3.3 g/s) are shown in Fig. 10. Finally, data resulting from test conditions of $U_\infty = 40$ m/s with $C_\mu = 0.0032$ and 0.0036 ($Q_m = 3.3$ and 3.7 g/s) are shown in Fig. 11. Figures 9–11 indicate the influence of different blowing mass flow rates on the oscillations of the vortex breakdowns, as well as the effectiveness of the flow control to displace aft the mean vortex breakdown locations.

Figure 12 is a graph of the time-averaged X_b/c values calculated from the data shown in Figs. 4 and 9–11. This graph is useful for comparing the time-averaged effects of varying C_μ on the position of vortex breakdown locations at various test conditions, as well as the changes to the rms values of the oscillating breakdown locations due to flow control. To facilitate the interpretation of the data, lines connect the portside and starboard mean X_b/c positions at corresponding test conditions and values of C_μ.

The first of the plots in Fig. 9 (Fig. 9a) demonstrates the effectiveness of blowing along the portside vortex core to displace aft the portside vortex breakdown location. In this case, the blowing momentum coefficient is not high enough to displace the vortex breakdown position aft of the trailing edge of the wing at all times, and large amplitude oscillations are evident in the data. Comparing this plot to Fig. 4a, one observes that the X_b/c values have been increased more than 20% of the root chord, indicating a displacement of the breakdown of over 20%. The mean X_b/c and rms values from Fig. 12 likewise show these trends. The displacement of the mean X_b/c between the cases for $C_\mu = 0$ and 0.009 is over $0.2 \times X_b/c$, whereas the respective rms value more than doubles, indicating the large-amplitude oscillations. Interestingly, the mean X_b/c of the starboard vortex has moved slightly closer to the apex of the delta wing, indicating a negative influence of asymmetric blowing and an interaction between the two leading-edge vortices (Fig. 12). The rms value of the starboard side has also been slightly reduced, which denotes increased stability in the starboard vortex breakdown locations as a result of portside along-the-core blowing.

The second plot in Fig. 9 (Fig. 9b) shows that, by increasing C_μ to 0.03 along the portside vortex, the portside vortex breakdown is permanently displaced aft of the trailing edge of the delta wing. The straight line at $X_b/c = 1$ represents the vortex breakdown position

at or downstream of the trailing edge because no point of reference exists to track the vortex breakdown location beyond the trailing edge of the wing. Data in Fig. 12 confirm these observations in that the portside mean $X_b/c = 1$, whereas the portside rms value is at zero, because the data do not fluctuate. As in the results for $C_\mu = 0.009$ along the portside vortex, the starboard mean X_b/c is slightly upstream of the no-blowing case when $C_\mu = 0.03$. The rms value of the starboard breakdown location, however, does not change significantly in this case.

The two plots in Fig. 10 also demonstrate the effectiveness of blowing along the core of the portside vortex to displace aft the portside vortex breakdown location. In the first plot of Fig. 10 (Fig. 10a), C_μ is equal to 0.005 and, as one would expect, it is not high enough to displace the vortex breakdown position aft of the trailing edge of the wing at all times. As in Fig. 9a, this level of the blowing momentum coefficient induces large-amplitude oscillations and manages to displace the portside vortex breakdown location downstream more than 20% of the root chord. The mean X_b/c and rms values from Fig. 12 denote these trends as well. The displacement of the mean X_b/c between the cases for $C_\mu = 0$ and 0.005 is over $0.2 \times X_b/c$, whereas the respective rms value more than doubles. As in the preceding case, the mean X_b/c of the starboard vortex has moved slightly closer to the apex of the delta wing, indicating a negative influence of asymmetric blowing and an interaction between the two leading-edge vortices (Fig. 12). The rms value of the starboard side has also been slightly reduced, which denotes increased stability in the starboard vortex breakdown locations as a result of portside along-the-core blowing.

The second plot in Fig. 10 (Fig. 10b) shows that, by increasing C_μ to 0.009 along the portside vortex, the portside vortex breakdown is permanently displaced aft of the trailing edge of the delta wing, as denoted by the straight line at $X_b/c = 1$. It is interesting to note that this is the same blowing momentum coefficient represented in Fig. 9a, which did not permanently displace the portside breakdown location downstream of the trailing edge. The only differences between these two tests are the freestream velocities ($U_\infty = 15$ m/s in Fig. 9 and $U_\infty = 24$ m/s in Fig. 10) and the blowing mass flow rates ($Q_m = 1.4$ g/s in Fig. 9 and $Q_m = 3.3$ g/s in Fig. 10). From these results, it appears that C_μ may not be a good nondimensional coefficient on which to base the results of along-the-core blowing. Again, the portside rms value is almost zero because the data are in virtually a straight line. In this case, both the starboard mean X_b/c and the rms value of the starboard breakdown location are not significantly different from those of the nominal case.

Because of maximum pressure limitations with the compressed air supply, the blowing momentum coefficients at $U_\infty = 40$ m/s are much lower than for the test conditions at $U_\infty = 15$ and 24 m/s, although the values of the blowing mass flow rates remain approximately the same. The first plot in Fig. 11 (Fig. 11a) represents data for $C_\mu = 0.0032$ ($Q_m = 3.3$ g/s), and the second plot (Fig. 11b) contains data for $C_\mu = 0.0036$ ($Q_m = 3.7$ g/s). On the basis of the two preceding examples, one would expect these blowing momentum coefficients to have little influence on the leading-edge vortex breakdown locations. Surprisingly, the two plots in Fig. 11 and their corresponding data in Fig. 12 mirror the results shown in Figs. 9 and 10 and their respective data in Fig. 12. The analysis describing the data from Fig. 9 at $U_\infty = 15$ can be applied directly to the results denoted in Fig. 11. For the case where $C_\mu = 0.0032$, the portside mean X_b/c is displaced downstream approximately 12% of the root chord, whereas for $C_\mu = 0.0036$, the portside mean X_b/c is displaced aft of the trailing edge except for a few seconds at the beginning of the sampling time (Fig. 12). The starboard mean X_b/c is displaced upstream for both cases. Likewise, the rms value for the portside data increases for the lower value of C_μ and becomes significantly smaller for $C_\mu = 0.0036$; however, the rms value remains relatively high in this case due to the oscillations that occur during the first 5 s of the data. In both these cases, the starboard rms values are lower than in the nominal no-blowing case.

The general trend of asymmetric blowing along the portside vortex core is to displace downstream the portside X_b/c toward the trailing edge of the wing. All of the data in Figs. 9–11 denote the ability of portside blowing along the leading-edge vortex core to displace aft the mean portside X_b/c more than 20% of the root chord; therefore, this asymmetric flow control is effective for controlling the vortex breakdown location over a delta wing. However, the orientation of the jet's flow and the mechanism of its influence on the leading-edge vortices are not well understood and are the subject of current studies at ONERA.

While the portside vortex breakdown location is displaced aft, the mean starboard X_b/c is shifted farther upstream with portside blowing than it is under the nominal no-blowing case, indicating both an influence from the asymmetric flow control and an interaction between the two leading-edge vortices. These leading-edge vortex interactions and the effects of asymmetric control systems are not well understood because only a few papers have addressed asymmetric blowing, either at or near the apex or at the trailing edge.[43] Another important question raised during this effort involves the ability of tangential blowing to stabilize the vortex breakdown locations. Helin[43] stated that the use of two symmetric trailing edge jets could both stabilize and delay the breakdown location of the primary vortices. Only one jet was used over the wing models in this study, and therefore symmetric blowing was not attainable.

Steady Surface Pressure with Blowing

Figure 13 consists of a plot of constant pressure coefficient lines at $U_\infty = 24$ m/s for $\alpha = 27$ deg, with $C_\mu = 0.009$. The influence of

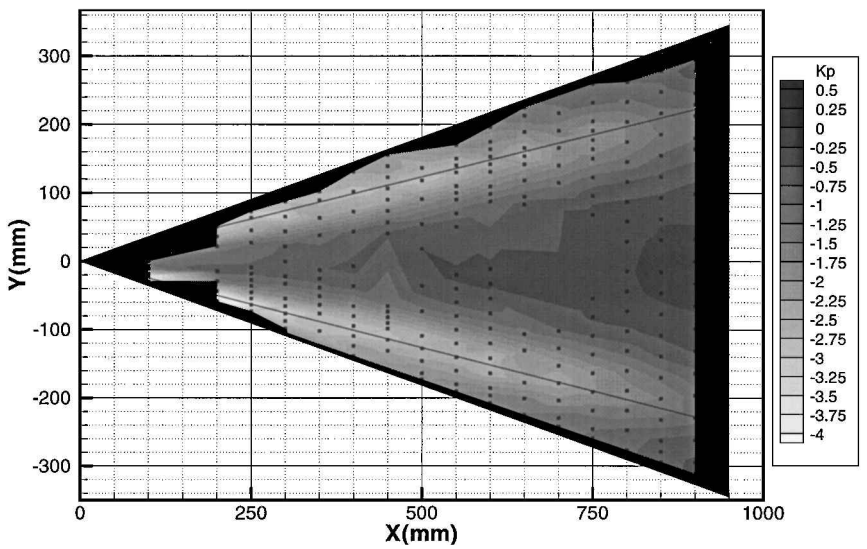

Fig. 13 Lines of constant-pressure coefficient on the leeward surface at $\alpha = 27$ deg for $U_\infty = 24$ m/s with $C_\theta = 0.009$.

blowing along the portside leading-edge vortex is clear when comparing Figs. 8 and 13. There are minor changes to the lines of the constant-pressure coefficient in the forward 50% of the wing where the pressure coefficients attain their highest negative values and most directly influence the lift of the wing. There are slight changes in the pressure coefficients measured at $X = 300$ mm, and the region of constant $C_p = -3$ is slightly more defined due to the open-loop blowing. However, C_p is reduced along the portside vortex core for the aft half of the delta wing due to the flow control. The two most significant changes occur for lines of constant $C_p = -2.75$ and -2.5, which have been extended aft 5 and 10% of the chord, respectively. The changes in C_p on the starboard side of the delta wing are minimal. Therefore, the influence of flow control has an impact on the coefficients of pressure on the portside of the wing and very little effect on the C_p on the uncontrolled, starboard side. Unfortunately, there is still no reliable indication that the time-averaged vortex breakdown location has been shifted downstream of the trailing edge of the delta wing, which is evident in the flow visualization data at this C_μ.

Conclusions

The unique data presented concerning oscillating vortex breakdown location at higher Reynolds numbers and the resulting evaluation of the Strouhal number and statistical data will help describe the vortex breakdown locations and permit a more exact examination of the effects of various flow control methods. The spectral analysis of oscillating vortex breakdown location showed that the principal frequencies at these higher Reynolds numbers (Strouhal numbers from 0.04 to 0.07) are similar to those determined at much lower Reynolds numbers (Strouhal numbers from 0.05 to 0.09). Thus, these results quantitatively confirm the results of qualitative visualization studies that indicate that the vortex breakdown phenomena over slender, sharp-edged, delta wings are insensitive to Reynolds number.

Open-loop, asymmetric, blowing along the core of the portside leading-edge vortex on the leeward surface of the delta wing was shown to be effective for controlling the vortex breakdown location over a delta wing. This asymmetric flow control technique demonstrated the ability to displace aft the portside vortex breakdown location more than 20% of the root chord at various test conditions. While the portside vortex breakdown location is displaced downstream with portside blowing along the vortex core, the mean starboard X_b/c is shifted farther upstream than under nominal no-blowing configuration. Therefore the asymmetric flow control influences both the controlled and uncontrolled leading-edge vortices, denoting an interaction between the two leading-edge vortices. The asymmetric flow control also affected the stability of both leading-edge vortices and therefore provides additional insight into the interactions that exist between them.

Acknowledgments

The authors thank U.S. Air Force Research Laboratory/Air Force Office of Scientific Research for sponsoring the U.S. Air Force Engineer and Scientist Exchange Program that resulted in this international cooperative effort. The authors also express their sincerest thanks to the members of the S2Ch wind-tunnel team who helped make these tests a reality. We also thank the reviewers for their suggestions.

References

[1]Délery, J., "Physics of Vortical Flows," *Journal of Aircraft*, Vol. 29, No. 5, 1992, pp. 856–876.

[2]Werlé, H., "Sur l'Éclatement des Tourbillons," ONERA, Note Technique 175, Châtillon, France, Nov. 1971.

[3]Wentz, W. H., Jr., and Kohlman, D., "Vortex Breakdown on Slender Sharp-Edged Wings," *Journal of Aircraft*, Vol. 8, No. 3, 1971, pp. 156–161.

[4]Hall, M. G., "Vortex Breakdown," *Annual Review of Fluid Mechanics*, Vol. 4, 1972, pp. 195–218.

[5]Leibovich, S., "The Structure of Vortex Breakdown," *Annual Review of Fluid Mechanics*, Vol. 10, 1978, pp. 221–246.

[6]Sarpkaya, T., "On Stationary and Traveling Vortex Breakdowns," *Journal of Fluid Mechanics*, Vol. 45, Pt. 3, 1971, pp. 545–559.

[7]Nelson, R. C., "Unsteady Aerodynamics of Slender Wings," *Aircraft Dynamics at High Angles of Attack: Experiments and Modeling*, R-776, AGARD, 1991, pp.1-1–1-26.

[8]Délery, J., "Aspects of Vortex Breakdown," *Progress in Aerospace Sciences*, Vol. 30, 1994, pp. 1–59.

[9]Werlé, H., "Quelques Résultats Expérimentaux sur les Ailes en Flèche, aux Faibles Vitesses, Obtenus en Tunnel Hydrodynamique," *La Recherche Aérospatiale*, No. 41, Sept.–Oct. 1954, pp. 15–21.

[10]Peckham, D. H., and Atkinson, S. A., "Preliminary Results of Low Speed Wind Tunnel Tests on a Gothic Wing of Aspect Ratio 1.0," Aeronautical Research Council, CP 508, TN Aero 2504, April 1957.

[11]Elle, B. J., "On the Breakdown at High Incidences of the Leading Edge Vortices on Delta Wings," *Journal of the Royal Aero. Soc.*, Vol. 64, 1960, pp. 491–493.

[12]Werlé, H., "Sur l'Éclatement des Tourbillons d'Apex d'une Aile Delta aux Faibles Vitesses," *La Recherche Aéronautique*, No. 74, Jan.–Feb. 1960, pp. 23–30.

[13]Werlé, H., and Gallon, M., "Contrôle d'Écoulements par Jet Transversal," ONERA, Extrait de l'Aéronautique et l'Astronautique, No. 34, Paper 1972-2, 1972.

[14]Poisson-Quinton, P., "Contrôle du Décollement d'une Surface Portante par un Jet Transversal," Intervention au Congrès ICAS, Rome, Sept. 1970.

[15]Dixon, C. J., "Lift Augmentation by Lateral Blowing over a Lifting Surface," AIAA Paper 69-193, Feb. 1969.

[16]Cornish, J. J., "High Lift Applications of Spanwise Blowing," International Council of the Aeronautical Sciences, ICAS Paper 70-09, Sept. 1970.

[17]Bradley, R. G., and Wray, W. O., "A Conceptual Study of Leading-Edge Vortex Enhancement by Blowing," *Journal of Aircraft*, Vol. 11, No. 1, 1974, pp. 33–38.

[18]Campbell, J. F., "Augmentation of Vortex Lift by Spanwise Blowing," *Journal of Aircraft*, Vol. 13, No. 9, 1976, pp. 727–732.

[19]Seginer, A., and Salomon, M., "Augmentation of Fighter Aircraft Performance by Spanwise Blowing over the Wing Leading Edge," NASA TM-84330, March 1983.

[20]Visser, K. D., Iwansiki, K. P., Nelson, R. C., and Ng, T. T., "Control of Leading-Edge Vortex Breakdown by Blowing," AIAA Paper 88-0504, Jan. 1988.

[21]Magness, C., Robinson, O., and Rockwell, D., "Control of Leading-Edge Vortices on a Delta Wing," AIAA Paper 89-0999, March 1989.

[22]Iwanski, K. P., Ng, T. T., and Nelson, R. C., "An Experimental Investigation of Delta Wing Vortex Flow with and Without External Jet Blowing," AIAA Paper 89-0084, Jan. 1989.

[23]Miller, L. S., and Gile, B. E., "The Effects of Blowing on Delta Wing Vortices During Dynamic Pitching at High Angles of Attack," AIAA Paper 92-0407, Jan. 1992.

[24]Afchain, D., and Deluc, J. M., "Etude de l'Éclatement des Nappes Tourbillonnaire sur une Aile Delta de 70 Degrés de Flèche à 27 Degrés d'Incidence. Contrôle de l'Éclatement par Soufflage. Soufflerie F2," ONERA, Rapport Technique 54/1147 ANG, Fauga-Mauzac, France, Sept. 1992.

[25]Laval-Jeantet, R., "Contribution à l'Étude du Contrôle Actif de l'Éclatement Tourbillonnaire sur Aile en Flèche en Écoulement Incompressible," Ph.D. Dissertation, Université d'Aix–Marseille II, Marseille, France, March 1993.

[26]Kuo, C.-H., Lu, N.-Y., and Lin, D.-C., "Evolution of Vortical Structure over Delta-Wing with Transient Along-Core Blowing," *AIAA Journal*, Vol. 35, No. 4, 1997, pp. 617–624.

[27]Kuo, C.-H., and Lu, N.-Y., "Unsteady Vortex Structure over Delta-Wing Subject to Transient Along-Along Core Blowing," *AIAA Journal*, Vol. 36, No. 9, 1998, pp. 1658–1664.

[28]Guillot, S., Gutmark, E. J., and Garrison, T. J., "Delay of Vortex Breakdown over a Delta Wing via Near-Core Blowing," AIAA Paper 98-0315, Jan. 1998.

[29]Garg, A. K., and Leibovich, S., "Spectral Characteristics of Vortex Breakdown Flowfields," *Physics of Fluids*, Vol. 22, No. 11, 1979, pp. 2053–2064.

[30]Ayoub, A., and McLachlan, B. G., "Slender Delta Wing at High Angles of Attack–A Flow Visualization Study," AIAA Paper 87-1230, June 1987.

[31]Gad-el-Hak, M., and Blackwelder, R., "Control of the Discrete Vortices from a Delta Wing," *AIAA Journal*, Vol. 25, No. 8, 1987, pp. 1042–1049.

[32]Portnoy, H., "Unsteady Motion of Vortex-Breakdown Positions on Delta Wings," International Council of the Aeronautical Sciences, Jerusalem, 1988, pp. 1299–1303.

[33]Solignac, J.-L., Sarrazin, M., and Gallon, M., "Eclatement de Tourbillons d'Ailes Delta à Forte Incidence," ONERA, Rapport Technique 49/1147 AN, Châtillon, France, Oct. 1991.

[34]Solignac, J.-L., and Gallon, M., "Contribution de la Visualisation à l'Étude Instationnaire de l'Éclatement Tourbillonnaire," ONERA, TP 1992-93, Futuroscope de Poitiers, France, June 1992.

[35]Gursul, I., and Yang, H. "On Fluctuations of Vortex Breakdown Location," *Physics of Fluids*, Vol. 7, No. 1, 1995, pp. 229–231.

[36]Menke, M., Yang, H., and Gursul, I., "Further Experiments on Fluctuations of Vortex Breakdown Location," AIAA Paper 96-0205, Jan. 1996.

[37]Menke, M., and Gursul, I., "Self-Excited Oscillations of Vortex Breakdown Location over Delta Wings," AIAA Paper 97-0744, Jan. 1997.

[38]Gursul, I., "Unsteady Flow Phenomena over Delta Wings at High Angle of Attack," *AIAA Journal*, Vol. 32, No. 2, 1994, pp. 225–231.

[39]Chanetz, B., "Contribution à l'Étude Expérimentale et Théorique de l'Éclatement Tourbillonnaire en Air Incompressible," Ph.D. Dissertation, Université de Lyon, Lyon, France, Sept. 1986.

[40]Press, W. H., Teukolsky, S. A., Vetterling, W. T., and Flannery, B. P., "Fourier Transform Spectral Methods," *Numerical Recipes in Fortran*, 2nd ed., Cambridge Univ. Press, Cambridge, England, U.K., 1992, pp. 381–436.

[41]Greenwell, D. I., and Wood, N. J., "Determination of Vortex Burst Location on Delta Wings from Surface Pressure Measurements," *AIAA Journal*, Vol. 30, No. 11, 1992, pp. 2736–2739.

[42]Jupp, M. L., Coton, F. N., Green, R. B., and Galbraith, R. A. M., "An Analysis of a Pitching Delta Wing Using High Resolution Pressure Measurements," AIAA Paper 98-2743, June 1998.

[43]Helin, H. E., "Effects of Trailing-Edge Jet Entrainment on Delta Wing Vortices," *AIAA Journal*, Vol. 32, No. 4, 1994, pp. 802–804.

S. K. Aggarwal
Associate Editor